Marine Chemistry 253 (2023) 104268

Contents lists available at ScienceDirect

Marine Chemistry

journal homepage: www.elsevier.com/locate/marchem

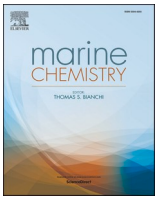

The solubility and deposition flux of East Asian aerosol metals in the East China Sea: The effects of aeolian transport processes

Chih-Chiang Hsieh [a,b], Chen-Feng You [c], Tung-Yuan Ho [a,b,*]

[a] Research Center for Environmental Changes, Academia Sinica, Taipei, Taiwan
[b] Institute of Oceanography, National Taiwan University, Taipei, Taiwan
[c] Department of Earth Sciences, National Cheng Kung University, Tainan, Taiwan

ARTICLE INFO

Keywords:
Trace metal
Size-fractionated aerosol
Solubility
Deposition flux
Transport process

ABSTRACT

Aerosol dissolvable metals are considered to be readily bioaccessible so that their input would influence the growth and composition of marine phytoplankton and affect elemental cycling globally. However, it is highly challenging to measure or estimate reliable deposition fluxes of aerosol dissolvable metals in the ocean partially due to the impacts of complicated processes involved in pre- and post-deposition of aerosols. We have collected lithogenic dust from major Chinese deserts and size-fractionated aerosols from the East China Sea (ECS) to study the variations of their dissolvable metals by using three operationally defined leaching protocols (ultrapure water, buffer, and Berger leaches). We have systematically investigated the changes of the distribution patterns of the metals to evaluate the potential impacts of the transport processes on the flux estimates of different elements. In addition to the extremely high solubilities observed for anthropogenic type elements, we found variations for solubilities of lithogenic type elements (Ti, Al, Fe) increase with increasing sizes by the three leaching treatments. Without knowing the size specific information (mass and solubility), our observations indicate that the deposition fluxes of lithogenic type elements would be significantly overestimated. Compared with the solubility of the desert dust, we found that all solubilities for lithogenic type elements in the largest aerosols were significantly enhanced. For example, the Fe solubilities increased up to 68, 6, and 3 folds for ultrapure water, buffer, and Berger treatments, respectively. Attributed to the difference of the impacts of the transport processes in different regions, the extent of the enhancement would be region specific. Comparing some other recent laboratory studies, we argue that the solubilities obtained by buffer and Berger leaches are more realistic to represent aerosol solubility in the ocean than ultrapure water leach. It would be essential to carry out similar field studies in other regions as this study to obtain region specific parameters of dissolvable aerosol metals to achieve better global modeling estimates on the fluxes of dissolvable aerosol metals in the ocean.

1. Introduction

The availability of the whole suite of biologically essential dissolved trace metals (e.g., Fe, Co, Cu, Zn, Ni) is a major factor deciding the growth and composition of different phytoplankton groups in marine euphotic zone (Chen et al., 2022; Ho et al., 2003; Paytan et al., 2009) and thus influencing material cycling in the ocean (Mackey et al., 2015; Martin and Fitzwater, 1988; Morel et al., 2020). Aerosols are a major source of dissolved trace metals in the euphotic zone of the ocean (Jickells et al., 2016). Before and after depositing in the euphotic zone, aerosols go through complicated atmospheric and aquatic physicochemical and transformation processes, such as acidification, photoreduction, and organic complexation (Meskhidze et al., 2019; Shi et al., 2012; Wang and Ho, 2020). Although the complicated processes would transform aerosol properties and influence aerosol metal solubilities (Longo et al., 2016; Takahashi et al., 2011), their impacts on the solubilities largely remain unclear (Meskhidze et al., 2019).

To mimic the impacts of the complicated physicochemical and transformation processes on aerosol metal solubilities, recent studies have suggested to standardize several typical leaching protocols for data compilation and flux estimate of the bioaccessible aerosol metals from different studies (Meskhidze et al., 2019; Perron et al., 2020). Bioaccessible aerosol metals are commonly and operationally defined as dissolved and labile fractions (Meskhidze et al., 2019). Reflecting

* Corresponding author at: 128, Sec. 2, Academia Rd., Nankang, Taipei 115, Taiwan.
E-mail address: tyho@gate.sinica.edu.tw (T.-Y. Ho).

https://doi.org/10.1016/j.marchem.2023.104268
Received 24 January 2023; Received in revised form 16 May 2023; Accepted 13 June 2023
Available online 16 June 2023

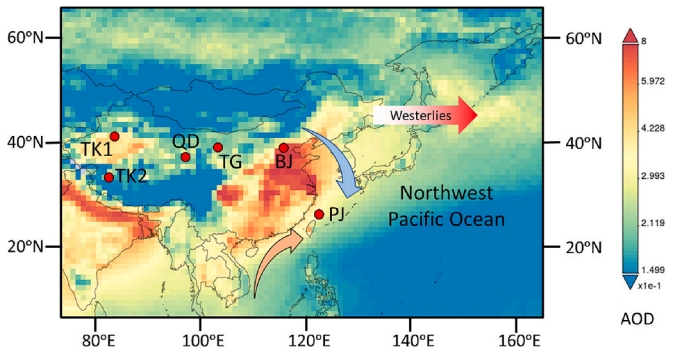

Fig. 1. The location of aerosol and dessert dust sampling sites of this study with aerosol optical depth as background. The annual averaged data of aerosol optical depth (2002–2022) are obtained by NASA Giovanni software (https://giovanni.gsfc.nasa.gov/giovanni/). The abbreviated letters, PJ, BJ, TK1, TK2, TG, and QD, stand for the sampling stations of aerosol samples or desert dust at Penjia islet, Beijing (NIES CRM No. 28), Taklimakan Desert, Taklimakan Desert, Tengger Desert, and Qaidam Desert, respectively.

instantaneously dissolved aerosol metals in the surface ocean, the dissolved fraction is obtained by passing ultrapure water through 0.2 or 0.45 μm aerosol filters (hereafter ultrapure water leach) (Buck et al., 2006; Morton et al., 2013) and considered to be fully bioavailable to phytoplankton (Raiswell and Canfield, 2012). To assess the labile fraction, acetate buffer (hereafter buffer leach) and Berger leaches are two of the most commonly used protocols. Buffer leach generally uses ammonia acetate buffer solution at pH 4.7 to mimic aerosol metals dissolution processes through atmospheric transport processes, such as the impacts of rainwater (Baker and Jickells, 2006; Sarthou et al., 2003) or short period ligand complexation in seawater (Perron et al., 2020). The Berger leach uses much stronger agents to release soluble metals, leached with acetic acid plus hydroxylamine hydrochloride for a fixed period of time, e.g., 1 day (Berger et al., 2008). The solubility obtained by Berger leach is thus considered as the upper limit of aerosol metals solubility in marine environment (Meskhidze et al., 2019; Shelley et al., 2018). It has been proposed that the solubility of Berger leach may represent the dissolvable fraction in aeolian metals through the acidification and reduction in zooplankton's gut, complexation by strong ligands (e.g., siderophores), and reduction in the microenvironment (Berger et al., 2008; Meskhidze et al., 2019).

In addition to accessing aerosol metal solubilities during transport processes by using different leaching protocols, the other major

Table 1
The mass fraction of the 5 size-fractionated aerosols and the averaged deposition velocities estimated by using fine, coarse, or 5-size aerosols collected in this study.

Element	Fraction	Elemental mass fraction (*w*/w, %)					Average deposition velocity		
		Size cut-offs (μm)					($cm\ s^{-1}$)		
		0.57	1.0	1.6	3.1	7.3	Fine	Coarse	5-size*
Cd	Ultrapure	43	27	14	9.3	6.5	0.023	0.87	0.16
	Buffer	42	27	15	8.9	7.2	0.024	0.89	0.16
	Berger	42	29	14	8.1	6.9	0.023	0.90	0.16
	Total	41	27	14	9.4	8.8	0.023	0.92	0.19
Zn	Ultrapure	37	25	16	13	9.5	0.025	0.88	0.21
	Buffer	32	26	15	13	14	0.026	0.94	0.27
	Berger	32	27	14	14	14	0.025	0.94	0.28
	Total	28	25	15	16	17	0.027	0.94	0.33
Pb	Ultrapure	57	25	8.8	6.2	3.3	0.019	0.83	0.10
	Buffer	45	25	12	9.1	8.8	0.022	0.93	0.18
	Berger	43	26	11	10	10	0.021	0.93	0.20
	Total	41	23	11	12	13	0.022	0.94	0.25
Mn	Ultrapure	25	14	16	25	20	0.030	0.90	0.42
	Buffer	22	14	16	24	24	0.032	0.93	0.46
	Berger	17	15	15	26	26	0.032	0.93	0.50
	Total	13	12	15	28	32	0.036	0.95	0.58
Co	Ultrapure	28	10	14	28	19	0.028	0.87	0.43
	Buffer	21	12	17	25	25	0.033	0.93	0.48
	Berger	16	10	13	28	33	0.033	0.96	0.60
	Total	10	9.5	15	32	34	0.039	0.94	0.63
Ni	Ultrapure	71	7.6	5.8	10	6.3	0.015	0.86	0.15
	Buffer	60	12	7.9	10	11	0.018	0.95	0.21
	Berger	54	11	7.4	11	17	0.018	1.0	0.29
	Total	36	11	10	19	24	0.022	0.97	0.43
V	Ultrapure	82	13	2.8	1.8	1.0	0.013	0.83	0.04
	Buffer	72	16	4.8	4.2	3.5	0.015	0.90	0.08
	Berger	59	13	7.8	10	11	0.018	0.94	0.21
	Total	30	10	11	22	27	0.025	0.96	0.49
Al	Ultrapure	59	16	14	9.1	2.3	0.021	0.73	0.10
	Buffer	36	12	15	23	14	0.026	0.84	0.33
	Berger	17	9.3	15	24	34	0.034	0.99	0.59
	Total	8.2	8.3	13	31	39	0.039	0.97	0.69
Fe	Ultrapure	59	21	10	7.4	2.8	0.019	0.78	0.10
	Buffer	32	17	13	18	20	0.026	0.94	0.38
	Berger	11	14	17	27	31	0.037	0.95	0.57
	Total	3.6	6.8	13	33	44	0.046	0.98	0.76
Ti	Ultrapure	49	24	11	10	6.4	0.021	0.86	0.16
	Buffer	26	14	12	20	28	0.027	0.98	0.49
	Berger	13	11	16	23	38	0.036	1.0	0.63
	Total	2.9	6.0	12	31	48	0.047	1.0	0.80

* The averaged velocity is obtained by size specific solubility and mass from the 5-size fractions obtained in this study. Same approach is applied to the fine and coarse fractions.

challenge is to quantify the deposition fluxes of aerosol dissolvable metals to the surface ocean (Baker et al., 2016; Jickells et al., 2005; Mahowald et al., 2005). As aerosol sizes strongly influence their deposition velocities and also reflect their sources, aerosol sizes are highly associated with the deposition fluxes of dissolvable aerosol metals. Moreover, the impacts of aeolian transport processes on aerosol metal solubility are also associated with surface area to volume ratios in aerosols (Baker and Jickells, 2006). However, most likely due to limited sampling time to collect sufficient aerosol masses in scientific cruises, many previous aerosol flux studies have only collected total suspended aerosol samples in the remote ocean. Attributed to the spatial deviation of aerosol size distribution and their composition and transport processes, the deposition fluxes of aerosol metals are likely to be element specific and also location specific. For example, the study of Hsieh et al. (2022) observed that the Fe solubilities of size-fractionated aerosols either for ultrapure water or buffer leaches showed difference up to two orders of magnitude between the finest and coarsest aerosols. Without using size-fractionated aerosols and their size-specific solubilities and deposition velocities, dissolvable Fe flux would be greatly overestimated (Hsieh et al., 2022). To obtain the reliable deposition fluxes of dissolvable aerosol metals and to reduce the uncertainties of the estimated fluxes by models, it is essential to obtain the distribution patterns of elemental concentrations in different size aerosol fractions by using different leaching protocols at major oceanic regions (Foret et al., 2006).

The East China Sea (ECS) is located at the downwind side of mainland China, a major aerosol source to the global ocean. The ECS receives a large amount of aerosols mixed with relatively fine anthropogenic aerosols and coarse lithogenic dust, originating from the populous Eastern China (Cheng et al., 2012) and Western China with major deserts, respectively (Fig. 1). During the northeastern monsoon and the Westerly prevailing periods, generally ranging from October to early May, the mixed aerosols accompanying with other pollutants (e.g., inorganic acids) are transported to the ECS, the adjacent marginal seas, and the Northwestern and subarctic Pacific Oceans. Contrarily, during the southwestern (SW) monsoon season from June to September, the ECS mainly receives aerosols originating from the South China Sea and Southeastern Asia. The ECS thus provides an excellent platform to study how aerosol metal solubility is affected by the natural transport process and the interaction with anthropogenic pollutants.

In this study, we have collected both lithogenic dusts directly from major Chinese deserts, including Taklimakan and Gobi Deserts, and the size-fractionated aerosols from the ECS to investigate the potential effects of transport processes and aerosol sizes on aerosol metal solubilities and deposition fluxes. We have systematically determined the solubilities of ultrapure water, buffer, and Berger leached metals and their corresponding deposition velocities among five different size-fractionated aerosols collected at Pengjiayu (PJ), a small islet located in the ECS, for one year. We have evaluated the discrepancy of the deposition velocities for different elements among the leaching treatments and the bias of flux estimates from a single velocity obtained by total suspended particle data. The findings of this study shall provide useful information for how to obtain a more representative estimate of the deposition fluxes of dissolvable aerosol metals regionally and globally.

2. Method

2.1. Sampling sites and method

For desert dust, the samples were directly collected from the land surface of three major Chinese deserts, Tengger Desert (TG, part of Gobi Desert, at 39°00′N, 103°34′E), Taklimakan Desert (TK1, at 36°48′N, 82°16′E; TK2, at 41°04′N, 83°29′E), and Qaidam Desert (QD, at 37°20′N, 97°09′E) (Fig. 1). The desert samples serve as the original lithogenic dust without being impacted by aeolian transport processes. The ECS aerosol sampling site, Pengjiayu (PJ, 25.63°N, 122.08°E), is located at 66 km from the northernmost point of Taiwan (Fig. 1). Except for limited governmental staff from Central Weather Bureau and Coastal Guard Administration, there are no other general residents or any other anthropogenic activities on the islet. The top of the volcanic islet, with area of 1.1 km^2, is mainly covered with grasses. PJ thus serves as an ideal aerosol time series sampling site for the East China Sea. Set up right next to the weather station of Central Weather Bureau on PJ, the high volume aerosol sampler (TISCH Environmental Inc., US, MODEL-TE-5170) was coupled with a cascade impactor (TISCH Environmental Inc., US, Series 235) to collect size-fractionated aerosol samples with average flow rate to be 1.0 ± 0.1 m^{-3} min^{-1}. The cascade impactor sorted aerosols into five size fractions, including stage 1 (>7.3 μm), stage 2 (3.1–7.3 μm), stage 3 (1.6–3.1 μm), stage 4 (1.0–1.6 μm), and stage 5 (0.57–1.0 μm) (Table 1). Size-fractionated aerosol samples were collected by polytetrafluoroethylene filters (TE-230-PTFE, Tisch Environmental Inc., US). Fine and coarse aerosols mentioned in this study refer to PM ≤ 3 (stage 3–5) and PM > 3 (stage 1 and 2), respectively. Since aerosol samples were not evenly distributed into 10 strips on each slotted filter in the impactor, we used the software ImageJ to measure the grayscale intensity value of each strip and summed up all strips in the whole filter. We then carried out total digestion or other leaching treatments by using one of the strips to calculate the concentrations of each strip and the whole filter by using the ratios of the intensities. To collect sufficient masses for the measurement of elemental and isotopic composition for different treatments, aerosols were continuously collected for 7–8 days on one filter every month from September 2019 to August 2020. As the sampler was under maintenance in October and November in 2019, data are not available for the two months. Aerosol samples were stored in a −20°C freezer before further chemical processes. Right before the chemical processes, each filter was freeze-dried and weighed.

2.2. Leaching procedures and quantification of aerosol metals

We have followed the procedures suggested in the GEOTRACES Cookbook to process aerosol samples and to clean vials used for sample storage and digestion (Cutter et al., 2017). All acids and bases used for sampling pretreatment were ultra-high purity grade, including nitric acid (HNO_3), hydrochloric acid (HCl), hydrofluoric acid (HF), acetic acid (CH_3COOH), ammonium hydroxide (NH_4OH)(J. T. Baker), except hydroxylamine hydrochloride ($NH_2OH.HCl$), which was high purity grade (>99%, Merck). Aerosol filters were sub-sampled with a trace metal clean ceramic scissor for different leaching treatments. All of the laboratory procedures were carried out in a positive pressurized class 5 cleanroom by wearing powder-free polyvinyl chloride (PVC) gloves while handling sample pretreatment procedures.

In addition to total digestion, we conducted three different leaching protocols, including instantaneous ultrapure water, acetate buffer (buffer), and Berger treatments. The ultrapure water leach was obtained by immersing aerosol samples in 5 mL of ultrapure water (> 18.2 MΩ. cm) with gentle shaking for 10 s. The leaching solution was then filtered into a pre-acid washed 15 mL polypropylene vial through a 13 mm pre-acid washed 0.2 μm hydrophilic PTFE syringe filter (Advantec) (Sarthou et al., 2003). Samples for buffer leach were soaked in 8 mL of ammonium acetate (1.4 M, pH 4.7) at room temperature for 1 h (Baker and Jickells, 2006). Samples for Berger leach were heated at 90°C (heater temperature) for 10 min with 5 mL leaching solution containing 25% acetic acid and 0.02 M hydroxylamine hydrochloride in PFA vials (Savillex)(Berger et al., 2008). The leaching treatment was maintained at room temperature for 24 h before further processes. Samples for total digestion were heated for 4 h at 120°C (heater temperature) in 2 mL of a freshly prepared mixed solution containing 4 M HF, 4 M HCl, and 4 M HNO_3 (Eggimann and Betzer, 1976). For buffer leach, Berger leach, and total digestion, after removing the filters, the leaching or digested solution were centrifuged to remove insoluble particles (Baker et al., 2006; Sarthou et al., 2003). The supernatant was dried up with open caps then the dried samples were redissolved in 10 mL 0.5 M HNO_3 solution at

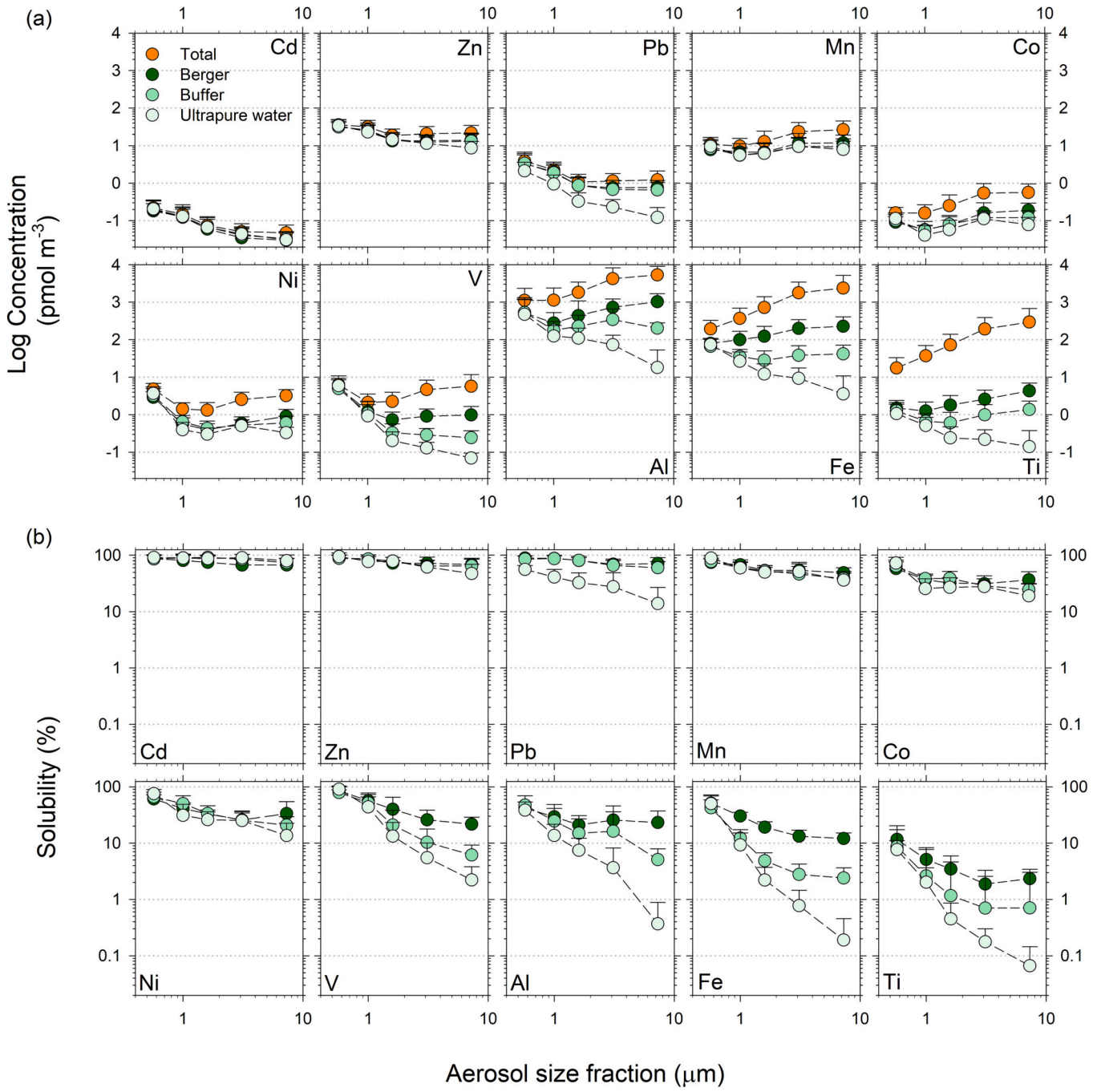

Fig. 2. The averaged elemental (a) concentrations and (b) solubilities obtained by ultrapure water, buffer, Berger and total digestion treatments in the size-fractionated aerosols collected at PJ. Light green, green, dark green and orange stand for the data of ultrapure water, buffer, Berger and total digestion treatments, respectively. Error bars stand for one standard deviation of all monthly data during the sampling period. (For interpretation of the references to colour in this figure legend, the reader is referred to the web version of this article.)

120°C (heater temperature) with closed caps for 1 h for further concentration quantification. The solubilities of the four leach fractions were calculated by dividing the leached concentrations to the total concentrations for individual elements. The filter blanks of each treatment were obtained by using new filters treated with exactly the same leaching procedures as samples. The concentrations of >90% of the samples were two orders of magnitude higher than the blank and all samples were one order of magnitude higher than the blank (Table S1).

All of the leached or digested samples were added with 1 ppb (final concentration) of indium and rhodium as internal standards and were diluted with 0.5 M HNO_3 solution accordingly, then were analyzed by a sector field high resolution ICPMS (Element XR, Thermo Fisher Scientific). The isotopes of ^{103}Rh, ^{111}Cd, ^{115}In, ^{207}Pb and ^{208}Pb were determined at low resolution (M/ΔM ~ 300), and ^{27}Al, ^{47}Ti, ^{49}Ti, ^{51}V, ^{55}Mn, ^{54}Fe, ^{56}Fe, ^{59}Co, ^{60}Ni, ^{64}Zn, ^{66}Zn, ^{103}Rh, and ^{115}In were analyzed at medium resolution (M/ΔM ~4000). In this study, we used two types of reference material for accuracy validation, including Arizona Test Dust (ATD, < 3 μm, Powder Technologies Inc.) to be lithogenic type CRM and NIES CRM No. 28, an urban aerosols collected in Beijing (BJ, National Institute for Environmental Studies), as anthropogenic type CRM. The ratios of our measured concentrations to the certified or reported value for ATD were 92% (Al), 100% (Ti), 102% (V), 92% (Mn), and 97% (Fe)

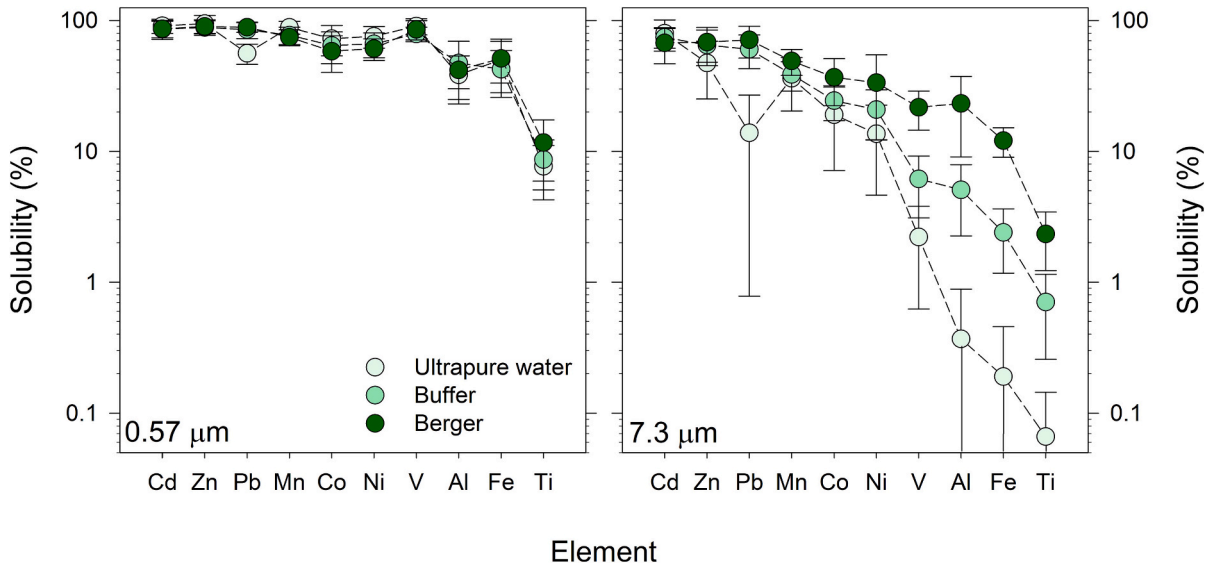

Fig. 3. The comparison of the elemental solubilities obtained by ultrapure water, buffer, and Berger treatments with the size cut-offs of 0.57 and 7.3 μm.

(Shelley et al., 2015); for BJ, 92% (Al), 93% (Ti), 101% (V), 95% (Mn), 97% (Fe), 125% (Co), 114% (Ni), 102% (Zn), 98% (Cd), and 99% (Pb) (Table S2).

3. Result

3.1. The variations of concentration and solubility

Fig. 2 shows the variations in concentrations and solubility of the metals obtained by three different leaching and digestion protocols for the size-fractionated aerosols. The monthly data of elemental concentrations (pmol m^{-3}) for the same size of particles by using relative standard deviations are compiled in Tables S3–S7. We present the elements from upper left to bottom right with low to high deviation sequences, which are Cd, Zn, Pb, Mn, Co, Ni, V, Al, Fe, and Ti (Fig. 2). Showing decreasing concentrations with increasing sizes, Cd and Zn exhibit the highest solubilities and smallest deviations among different protocols (Table S3). The average solubilities of ultrapure water, buffer, and Berger phases were 87, 86, and 80% and 72, 77, and 79% for Cd and Zn, respectively.

The concentration deviations of the elements, Pb, Mn, Co, and Ni, ranged between 39% and 72%, with the smallest deviation in the smallest size (0.57 μm) and increasing with sizes (Table S3). For the largest size aerosol, the difference of the concentrations was up to one order of magnitude among different leaching protocols. In terms of solubility, the average solubilities ranged from 17 to 81% and decreased with increasing sizes in all leaching fractions. For example, the average solubilities of Co for the ultrapure water, buffer, and Berger leaches were 73, 26, 27, 28, 19% and 64, 39, 39, 29, 24% and 58, 37, 32, 31, 37% for the aerosol fractions from small to large ones, respectively.

The third group of elements, including V, Al, Fe, and Ti, exhibit >90% of concentration deviations among the protocols (Table S3). The deviations were still relatively small for size 0.57 μm but were significantly deviated for large size aerosols, with deviations up to 3 orders of magnitude for 7.3 μm aerosols. In terms of solubility, the average solubilities of ultrapure water, buffer, and Berger leaches for the largest aerosols were 2.2, 6.1, 22% and 0.37, 5.1, 23% and 0.19, 2.4, 12% and 0.07, 0.70, and 2.3% for V, Al, Fe, and Ti, respectively.

To highlight the deviation patterns of the elemental solubilities among protocols and aerosol sizes, we present the deviations of the solubility of ultrapure water, buffer, and Berger treatments for the smallest and largest size aerosols (0.57 and 7.3 μm) with the sequence of deviation from low to high (Fig. 3). The average solubilities of 0.57 μm aerosol were all similarly high and >50% for most of the elements, with the values (average ± S.D.) to be 88 ± 13, 91 ± 12, 77 ± 18, 80 ± 12, 65 ± 18, 68 ± 14, 85 ± 13, 42 ± 17, 48 ± 19, and 9.3 ± 4.5% for Cd, Zn, Pb, Mn, Co, Ni, V, Al, Fe, and Ti, respectively (Fig. 3). For 7.3 μm aerosols, the deviation patterns of the solubilities were comparable to the deviation patterns of the concentrations among the three groups of elements mentioned above.

3.2. Enrichment Factor

Since aerosols are composed of multiple sources, the elemental ratios of metals can be significantly different from the composition in lithogenic dust. The enrichment factor (EF) of metals in aerosol samples may be useful to evaluate the relative contribution of the non-crustal sources. The enrichment factor (EF) is generally expressed as follows:

$$EF = (Metals/Ti)_{aerosol}/(Metals/Ti)_{UCC}$$

The term, $(Metals/Ti)_{UCC}$, stands for the reference value of the upper continental crust, which is cited from Hu and Gao (2008) in this study.

The EF of size-fractionated aerosol metals are shown in Fig. 4 and Table S8. Overall, the averaged EF of all sampling periods decrease with increasing sizes for all elements. In terms of the deviation of the EF in each size, Cd, Zn, Pb, Ni show relatively high variations, spanning up to one order of magnitude for most sizes. For example, the ranges for Cd were 199–3754, 67–1290, 12–317, 5.7–108, and 3.1–77 from the smallest to largest sizes, respectively. These high EF values indicate high anthropogenic aerosol contribution to the elements for all sizes. Even in coarse fractions, the average EF of Cd, Zn, Pb were significantly higher than 1, which are 32, 14, and 7.1, respectively. The coarse aerosol with high anthropogenic aerosol contribution might be attributed to coarse anthropogenic aerosols or the aggregation of fine anthropogenic aerosols on the coarse samples (Li et al., 2017). Seasonally, the average EF of Cd, Pb, and V were significantly higher ($p < 0.05$) during the NE monsoon period than the SW monsoon period (Fig. S1). Using Cd as an example, the EF value (average ± S.D.) with increasing sizes were 2025 ± 1024, 645 ± 451, 167 ± 112, 46 ± 28, 29 ± 20 and 364 ± 233, 110 ± 61, 28 ± 23, 11 ± 7.3, 6.7 ± 5.1 for the NE and SW monsoon seasons, respectively. All elements (except Zn) show significant seasonality in size 0.57 μm ($p < 0.05$).

For Al and Fe, the average EF values for the fine aerosols are 1.3 ± 1.2 and 1.8 ± 0.4, respectively. Even for the smallest size, the averaged EF are only 2.2 and 2.1 for Al and Fe, respectively. However, the

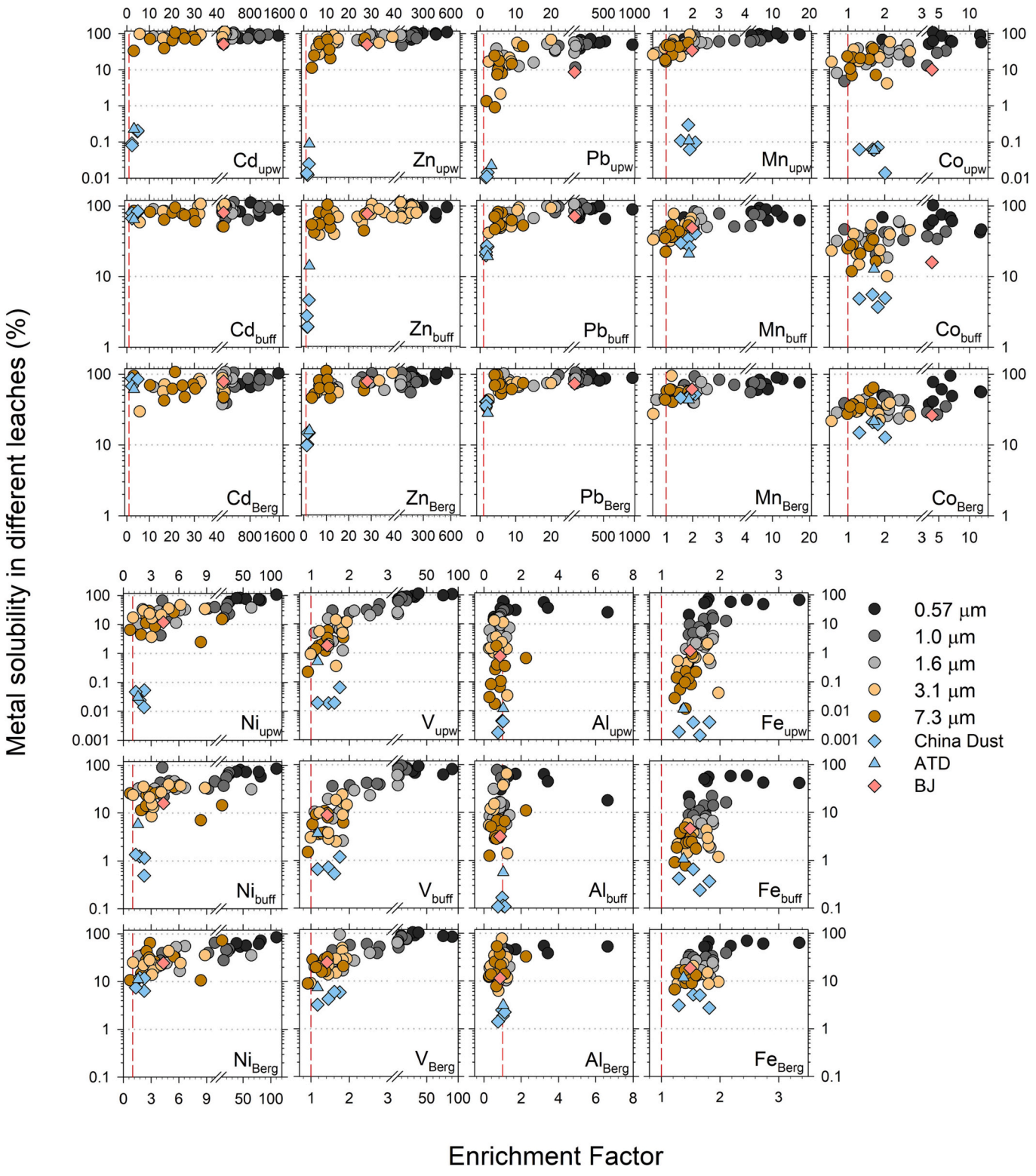

Fig. 4. The comparison of enrichment factors (EF) and the metal solubilities of size-fractionated aerosols and dust. The circle symbols stand for PJ aerosol samples, blue diamond for Chinese desert dust (China Dust), blue triangle for Arizona Test Dust (ATD), and red diamond for NIES CRM No. 28 Urban aerosols collected in Beijing (BJ). The numbers shown right next to the circle symbols are the size cut-offs of PJ aerosol samples. The three panels for each element stand for the results obtained by the three leaching methods, ultrapure water (upw), buffer (buff), and Berger leaches, respectively. (For interpretation of the references to colour in this figure legend, the reader is referred to the web version of this article.)

ultrapure water solubilities of fine aerosols for Al and Fe were extremely high, 38 and 50% (Fig. 4), indicating relatively high anthropogenic aerosol fractions in fine aerosols. The comparable EF between anthropogenic and lithogenic aerosols for Al and Fe indicates that EF is not a useful indicator to distinguish the relative contribution of crustal and non-crustal sources for Al and Fe.

4. Discussion

4.1. EF and leaching solubility

We found that the coupling of EF and solubilities may provide additional information to evaluate the sources of aerosols (Fig. 4). Using Al as an example, the EF of Al for the two extreme size aerosols (0.57 and 7.3 μm) are statistically indistinguishable, 2.2 ± 1.9 and 0.84 ± 0.55, but their averaged ultrapure water solubilities show dramatic difference up to two orders of magnitude, 38 ± 15 and 0.37 ± 0.52%, respectively. Normalized to the surface area of these two size aerosols, the Al solubility of 0.57 μm aerosols is still one order of magnitude higher than 7.3 μm aerosols. Thus, the extremely high ultrapure water solubility observed in the finest aerosols, whose EF is relatively close to 1, suggests that the soluble Al in the fine aerosols mainly originated from anthropogenic aerosols. Sakata (2022) also observed Al-sulfate and organic complexes in $PM_{1.3}$ of the Western Pacific Ocean aerosol, strongly supported our suggestion. Similarly, the EF of Fe for the two sizes of aerosols are 2.1 ± 0.6 and 1.4 ± 0.1, but the ultrapure water solubilities were 50 ± 22 and 0.19 ± 0.27%, respectively. We did observe correspondingly high solubilities in the fine aerosols with slightly higher EF for Fe, indicating that anthropogenic aerosols were also the major source of ultrapure water Fe in fine particles. For Cd, Zn, and Pb, their EF in almost all coarse aerosol samples were significantly higher than 1, and the solubilities were all relatively high. For Mn (and Co), the EF were mostly under 10. Although the EF values in fine and coarse particles were slightly different, 4.4 ± 4.0 and 1.3 ± 0.4, their ultrapure water solubilities were statistically insignificant, 65 ± 20 and 44 ± 21%, respectively. In brief, the Ti-normalized EF of Al, Fe, Mn, and Co in fine aerosols are either insignificantly different or just slightly higher than the EF in coarse aerosols in the samples. For Mn, Co, Ni, and V with EF smaller than 2, we observed high deviations of ultrapure water solubilities, ranging from 15 to 95, 4.2–59, 4.5–17, and 0.2–14%, respectively, indicating that the information of EF alone is impractical to be a useful proxy to evaluate the solubilities and the relative contribution of non-crustal source. For Cd, Zn, Pb, Ni, V, Mn and Co, the EF were up to 100 or even 1000, and their ultrapure water solubilities were all relatively high, with average solubilities for data with EF higher than 10 to be 86 ± 15, 77 ± 19, 45 ± 16, 59 ± 25, 90 ± 14, 92 ± 12, and 74 ± 23%, respectively. Overall, the coupling information of EF and solubilities serves as a much more reliable and useful indicator than EF itself to reflect the relative contribution of crustal and non-crustal sources on the ultrapure water metals in size-fractionated aerosols.

The comparison of the solubility obtained by the three leaching treatments for the size-fractionated aerosols exhibits elemental dissolution characteristics among aerosol sources. The results show that most metals in fine aerosols are released into water instantaneously (Figs. 2–4). Previous studies reported that anthropogenic type metals exist in highly soluble salts, mainly nitrate and sulfate, or complexed with organic ligands in aerosols (Sakata et al., 2014), which explains the high metal solubilities observed in fine aerosols. However, the ultrapure water fraction of Pb are significantly lower than other fractions, which may be attributed to the contribution of relatively insoluble forms, $2PbCO_3{\cdot}Pb(OH)_2$ and $PbSO_4$, in both fine and coarse aerosols (Sakata et al., 2017). In terms of lithogenic type elements (e.g., Al, Fe, and Ti) in the coarsest aerosol, their ultrapure water solubilities were extremely low, which are attributed to their relatively stable crystalline lattice structure in lithogenic aerosols (Nicholls, 1963). However, their buffer and Berger solubilities increased significantly in comparison to ultrapure water solubilities in the coarsest fraction (Fig. 3). Using ultrapure water and buffer leaches in aerosol samples collected in a Chinese city, Li et al. (2023) also reported that the solubility ratios of buffer and ultrapure water leaches were significantly higher for Al and Fe than other metals with high ultrapure solubilities.

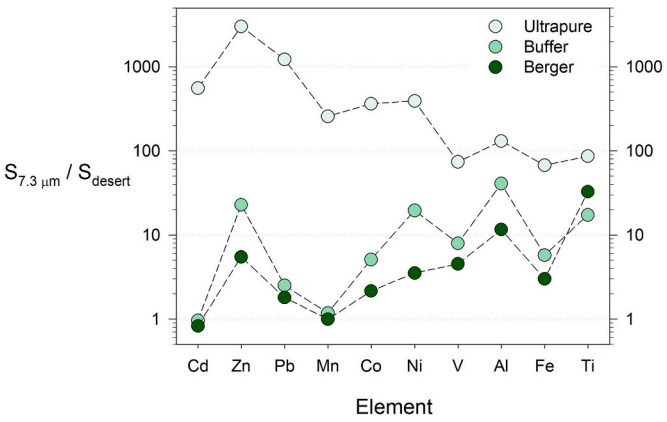

Fig. 5. The variation patterns of the solubility ratios between the aerosols (7.3 μm) to the Chinese dust for the three leaching treatments.

4.2. Reflecting the impacts of the transport processes on solubilities

We compile the solubility data between the desert dust (hereafter the dust in Section 4.2) and the largest size aerosols (size cut-off 7.3 μm, hereafter the aerosols in 4.2) to evaluate the potential impacts of aeolian transport processes on the three different solubilities of the largest aerosols collected (Fig. 4 and Table S9). Overall, except Cd, Zn, and Pb in the aerosols, the enrichment factors of the dust and the aerosols are both close to 1 for most of the elements measured (Fig. 4). The averaged EF of Cd, Zn, and Pb in the aerosols were up to 25, 12, and 5.9; and their averaged ultrapure water solubilities were 80, 47, and 14%, respectively. However, the ultrapure water solubilities of Cd, Zn, and Pb were extremely low in the dust, which were down to 0.14, 0.02, and 0.01%, respectively. The high EF and contrasting solubilities between the aerosols and the dust indicate that the largest aerosols are still mixed with a significant amount of Cd, Zn, and Pb originating from anthropogenic aerosols. For buffer and Berger leaches, the solubilities of Cd and Pb in the dust were significantly enhanced to 77 and 24% for buffer leach, and 81 and 39% for Berger leach, respectively, which are relatively close to the value observed in the aerosols. These significant solubility enhancements in the dust can be attributed to their relatively soluble composition in the dust. Using Cd as an example, the enhancement of solubility is likely caused by the most commonly found primary speciation in the dust, Cd oxides and sulfide (ATSDR, 1999), in which the solubilities are much higher in weak acid than in ultrapure water. Since buffer leach has been generally proposed to represent the effect of rainwater and organic ligand complexation fractions in seawater (Baker et al., 2006; Perron et al., 2020; Sarthou et al., 2003), these enhanced high solubilities observed in the dust indicate that the solubilities of Cd and Pb for lithogenic aerosols would be relatively high in rainwater or seawater. However, the averaged solubilities of the buffer and Berger leaches of the dust for Zn were 2.8 and 12%, respectively, which were significantly lower than the levels of Cd and Pb, most likely attributed to the relatively rigid mineral composition of Zn in the dust, such as willemite (zinc silicate) (Gunchin et al., 2021). Similar patterns for Mn, Co, Ni, and V are observed as Zn. Specifically, the effects of the three leaching treatments on Mn were close to the patterns of Cd and Pb. The buffer and Berger solubilities of Co, Ni, and V in the dust were significantly lower than the value observed in the aerosols. For Al and Fe, the instant solubilities for both the dust and the aerosols were both extremely low and relatively close to each other; the buffer and Berger

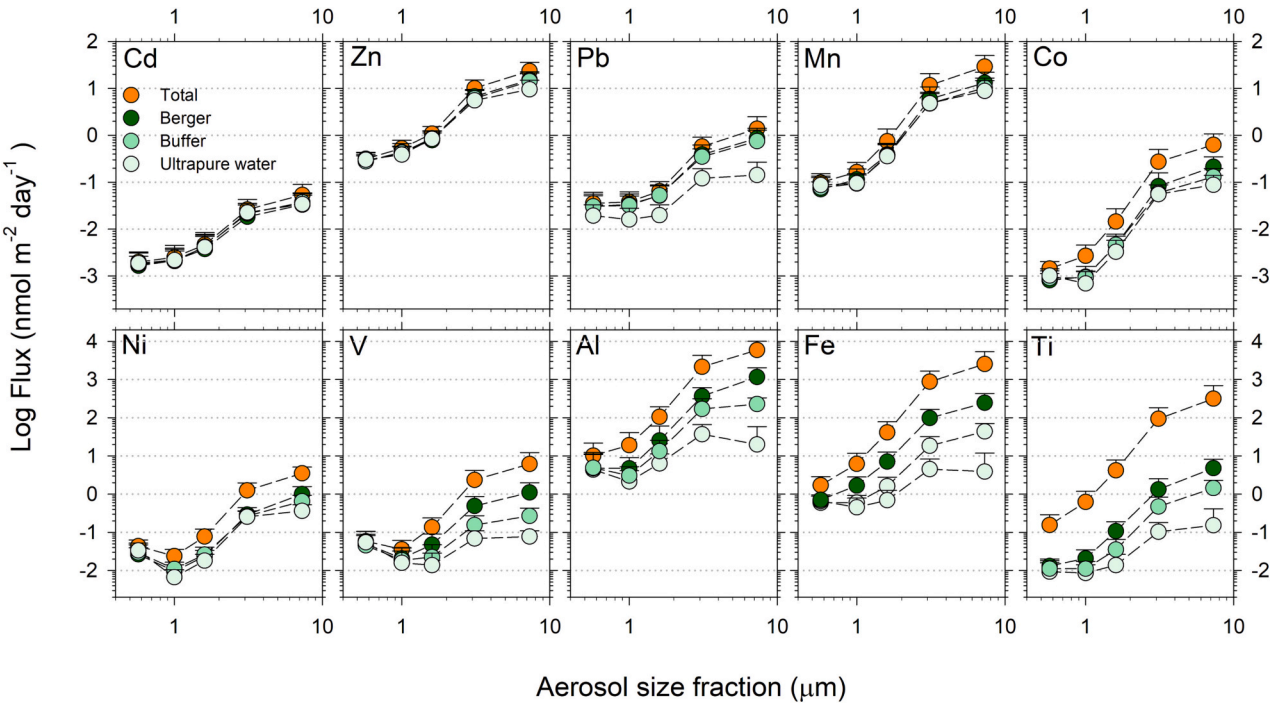

Fig. 6. The comparison of the averaged dry deposition fluxes estimated from the data obtained by ultrapure water, buffer, Berger, and total digestion treatments of the size-fractionated aerosol metals.

solubilities were significantly higher in the aerosols than the value observed in the dust.

We further present the solubility ratios between the aerosols to the dust ($S_{7.3\mu m}/S_{desert}$) from the three leaches together to illustrate the deviation patterns among all of the metals measured (Fig. 5). We found a converging trend of the ratios of the three leach treatments from anthropogenic to lithogenic type metals, which is defined as litho-tendency here for the elements measured. The ratios of ultrapure water leach decrease with litho-tendency with the value ranging from 3017 to 68. As pointed out previously, except Cd, Zn, and Pb, the low solubilities and EF (close to 1) in the aerosols indicate that the other metals are mostly lithogenic origin. The elevated ratios thus suggest that aeolian transport processes enhance ultrapure water solubilities of most elements significantly in the largest aerosols collected. Previous studies have reported that highly soluble metal salts are formed during transport processes with inorganic acids, such as sulfuric and nitric acid, from SO_2 and NO_x emissions, respectively. (Baker et al., 2021; Seinfeld and Pandis, 2016). By chemical reactions with the acids via in-cloud processes, the newly formed salts may include metal nitrate, sulfate, chloride, and organic complexes for Pb, Zn, and Mn (Ohta et al., 2006; Sakata et al., 2014; Takahashi et al., 2011), possibly for some other metals in the dust too. For ultrapure water treatment, the solubility ratios for Mn, Co, and Ni between the dust and the aerosol are significantly higher than V, Al, Fe, and Ti, suggesting the differentiated effects of transport processes on forming the readily soluble metal compounds in the dust.

On the other hand, the ratios of buffer and Berger leaches exhibit an increasing trend with elemental sequence from Cd to Ti, increasing with the litho-tendency and varying from around 1 to 35. The relatively low ratios observed in the Cd, Zn, and Mn were mainly attributed to highly enhanced solubilities caused by the buffer and Berger leaches for both the aerosols and the dust. For Co, Ni, V, Al, Fe, and Ti, the ratios of buffer and Berger leaches generally increase with the tendency. The deviations of the three ratios for Ti, the element with the highest litho-tendency, were down to be the same order of magnitude, which were 86, 17, and 33 for ultrapure water, buffer, and Berger treatments, respectively. In brief, the convergent patterns of the three ratios with the tendency reflect the coupling effects of the transport processes on the aerosols of a specific element under the leaching protocol (numerator) and the soluble behavior of any specific element in the dust under the leaching protocol (denominator). The converging tendencies and highly elevated ratios indicate that the transport processes enhance the solubilities of all elements under all leaching protocols and the enhancement extent is litho-tendency associated. In the other words, the transport impacts on the aerosols are element specific, which are partially attributed to the contribution of anthropogenic aerosol metals in the aerosols and partially attributed to the readiness of the metal composition in the aerosols to be solubilized during atmospheric transport processes.

4.3. *Element specific deposition velocity and flux*

Since both the solubilities and mass fractions are significantly different among different elements in size-fractionated aerosols (Fig. 2), the authentic deposition velocity of dissolvable aerosol metals shall be element specific. The accurate estimate of deposition flux for the dissolvable metals would thus require the information of the soluble mass among different sizes and their corresponding deposition velocities. For example, the deposition velocities of Fe for 5 size cut-offs vary up to 2 orders of magnitude, which are 0.008, 0.018, 0.063, 0.39, and 0.94 cm s^{-1} in the East China Sea, respectively (Hsieh et al., 2022). In addition to the importance of aerosol sizes, deposition velocity is also closely associated with aerosol density and atmospheric conditions, which are mainly decided by wind speed, relative humidity, and sea surface temperature (Slinn and Slinn, 1980).

Considering the velocities of each size fraction, we have calculated the deposition velocities of individual element for each size with ultrapure water, buffer, Berger, and total digestion treatments (Table 1). We have also calculated the deposition velocities for fine, coarse, and size-fractionated (5-size) aerosols based on the solubility and mass fraction data obtained in this study (Table 1). Using Cd as an example in anthropogenic type elements (Cd, Zn, Pb), due to its comparable mass fractions and high solubilities in all size fractions, the deposition velocities of Cd for same size aerosols are highly comparable among the four leaching or digestion treatments, which are 0.16, 0.16, 0.16, and

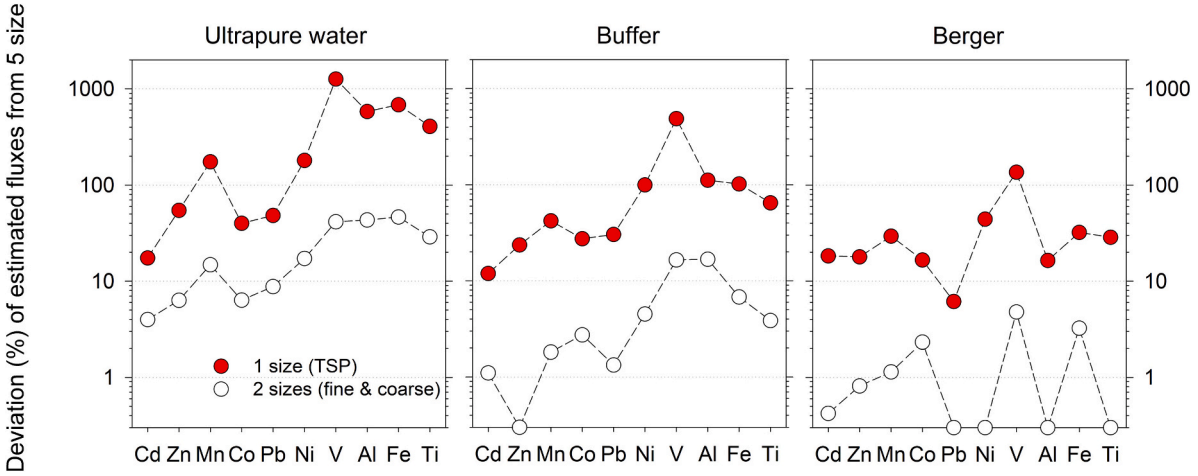

Fig. 7. The offset (or bias) of the deposition velocities obtained with one-size sampling (total suspended particles, TSP) with red circle symbol or with two-size sampling (fine & coarse) with open circle symbol to the velocities obtained by 5-size aerosol sampling for flux calculation. (For interpretation of the references to colour in this figure legend, the reader is referred to the web version of this article.)

0.19 cm s^{-1}, respectively. Similarly, the velocities are 0.21, 0.27, 0.28, and 0.33 cm s^{-1} for Zn, and 0.10, 0.18, 0.20, and 0.25 cm s^{-1} for Pb, respectively. The relatively low velocity of the ultrapure water treatment (0.10 cm s^{-1}) for Pb is attributed to its low percentage of coarse fraction (9.5%). On the other hand, the solubilities of lithogenic type elements vary dramatically among different size aerosols, particularly in coarse particles. Using Fe as an example, the relative mass fractions were 59, 21, 10, 7.4, 2.8%; 32, 17, 13, 18, 20%; 11, 14, 17, 27, 31%; and 3.6, 6.8, 13, 33, 44% for the four protocols, respectively. The mass fractions result in the deposition velocities to be 0.10, 0.38, 0.57, and 0.76 cm s^{-1} for the 4 treatments, respectively (Table 1). Similarly, the velocities are 0.10, 0.33, 0.59, and 0.69 cm s^{-1} for Al and 0.16, 0.49, 0.63, and 0.80 cm s^{-1} for Ti, respectively. The deviation of the 4 velocities for V is the highest among all elements, which are 0.04, 0.08, 0.21, and 0.49 cm s^{-1}, respectively, mainly attributed to its low percentage in coarse fraction for the ultrapure water and buffer treatments. Attributed to the high deviations among elements and the treatments, it is thus essential to obtain the soluble mass fraction information of size-fractionated aerosols for the accurate estimate of deposition velocities for individual element. The four velocities for both Mn and Co range from 0.42 to 0.63 cm s^{-1}, which are generally between the value of anthropogenic and lithogenic type elements (Table 1). Due to the comparable mass fractions among the four treatments, the deviations of the velocities are relatively small among the treatments, which are 0.42, 0.46, 0.50, and 0.58 cm s^{-1} for Mn and 0.43, 0.48, 0.60, and 0.63 cm s^{-1} for Co, respectively. The velocities for Ni are 0.15, 0.21, 0.29, and 0.43 cm s^{-1}, respectively. The relative contribution between anthropogenic and lithogenic aerosols in each size may differ spatially and result in region specific velocities for each element. Comparable studies in the adjacent regions of this study are needed to validate whether the deposition velocities reported in this study may represent the Northwestern Pacific Ocean. We suggest that more studies as what we have carried out in the ECS are also needed to obtain the spatially specific deposition velocities in other major oceanic regions.

Thus, without knowing the mass fraction information by different leaching treatments, the metal flux estimates from total suspended aerosols would overestimate the fluxes for all elements, except Cd. We have evaluated the bias of the deposition fluxes of dissolvable aerosol metals among three different size categories, 5 sizes, two sizes (fine and coarse), and 1 size (total) by using the following calculation.

$$F_{dry} = \sum_{i=1}^{5} C_i \times V_{d\_i} \text{ (or } C_F \times V_F + C_C \times V_C \text{ or } C_{TSP} \times V_{TSP})$$

The term, C_i, C_F, C_C, and C_{TSP} refer to the metal concentration of each leaching treatment in each size fraction. And V_{d_i}, V_F, V_C, and V_{TSP} represent the dry deposition velocities of each size range. Fig. 6 exhibits the variations and the deviations of the dry deposition fluxes by five different leaching and digestion protocols for the size-fractionated aerosols (Tables S10–S13). The extremely high deposition velocity in coarse aerosols is the major factor deciding the distribution patterns of the fluxes in size-fractionated aerosols. Overall, the fluxes of all elements increased with aerosol sizes even for the elements (e.g., Cd, Zn, and Pb) with relatively high concentrations in fine aerosols (Fig. 2). Using Cd as an example, the percentages of total Cd mass decreased with sizes, from 41 to 8.8% for the finest to coarsest aerosols but the total fluxes increased from 2.1 to 61%, respectively. The contribution of coarse aerosols to the total fluxes for all other elements are even higher. For V, Al, Fe, and Ti, the coarsest aerosol accounts for 63, 82, 82, and 89% in instant ultrapure water fluxes; 83, 95, 96, and 97% in buffer fluxes; 93, 98, 97, and 98% for Berger fluxes 97, 98, 99, and 99% in total fluxes, respectively (Tables S10–S13).

Previous oceanic studies on estimating the deposition fluxes of aerosol soluble metals are mainly based on total aerosol mass information. However, as shown in Table 1, the dissolvable fractions of different sizes vary significantly under different leaching protocols. We have estimated the offset or bias of the deposition fluxes between using the velocities obtained from one-size (total) or two-sizes (fine and coarse) and the velocities obtained from 5-size in this study (Table 1 and Fig. 7). The percentage of bias of ultrapure water metal fluxes are 54, 40, 48, 174, 180, 1266, 581, 682, 408% for Zn, Mn, Co, Pb, Ni, V, Al, Fe, and Ti, respectively (Fig. 7). The metals Pb, Ni, V, Al, Fe, and Ti have higher offsets for buffer metal fluxes estimates with bias to be 42, 100, 485, 111, 102, and 65%, respectively. The mass fraction of Berger leach is similar to the total treatment so only Ni and V have high offsets for flux estimates, with bias to be 39 and 123%, respectively. After the correction by multiple size aerosol collection mentioned above, two aerosol size sampling may significantly reduce the bias, with bias all within 50% for all leaching treatments and almost all elements with offset under 10% for buffer and Berger treatments (Fig. 7).

Although we did not collect wet deposition samples, it should be noted that wet deposition is important in our studied region. We have carried out a preliminary estimate on the wet deposition fluxes by using the proposed equation (Duce et al., 1991). The results are shown in Fig. S2.

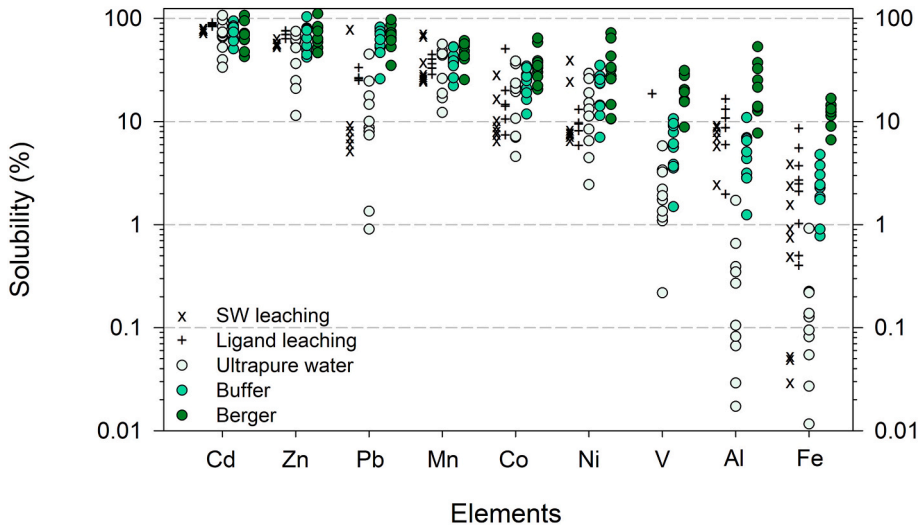

Fig. 8. The comparison of the solubilities obtained from ultrapure water, buffer, Berger leaching of the largest aerosols collected in PJ with seawater solubilities obtained in previous studies (Bonnet and Guieu, 2004; Félix-Bermúdez et al., 2020; Fishwick, 2014, 2018; Mackey et al., 2015) or by ligand leaching (Clough et al., 2019; Kessler et al., 2020; Wu et al., 2023.).

4.4. The implication to aerosol Fe flux estimate by models in the global ocean

The model accuracy for estimating global aerosol dissolvable metal fluxes to the ocean relies on the applicability of aerosol metal solubilities chosen in models. Although most of the global models, i.e., CAM4, GEOS-Chem, IMPACT, TM4-ECPL, have already considered the differences of the deposition velocities of multiple aerosol sizes (2–4 size bins) (Myriokefalitakis et al., 2018), the solubilities applied in those models did not clearly distinguish or consider the implications of the different solubilities obtained by the leaching treatments as shown in this study. The solubilities of aerosol metals can vary significantly and the variations are specific in aerosol sizes, leaching methods, and elements, especially for lithogenic type elements. For example, the ratios of dissolvable Fe concentrations (or solubility) by normalizing to ultrapure water leach for the three leaching treatment in bulk aerosols are 1: 1.6: 5.8, showing limited solubility difference between ultrapure water and buffer treatments (Tables S5–S7). However, the ratios in aerosol size 7.3 μm increased dramatically, with the ratios to be 1: 12: 64. Using long term seawater leaching or adding sufficient organic ligand approaches to lithogenic dusts, some recent laboratory studies also reported relatively high aerosol metal solubilities (Fig. 8). The solubilities of Fe and Al in many of these studies were comparable to the solubility levels observed by buffer and Berger leaches in this study (Fig. 8). For the model estimates of global aerosol dissolvable Fe fluxes, we argue that the solubilities obtained by buffer and Berger leaches are more realistic to represent aerosol Fe solubility in the ocean than the value obtained by ultrapure water leach.

5. Conclusion

This study demonstrates that solubilities obtained by different leaching treatments are highly varied for different metals in coarse aerosols. Thus, the impacts of transport processes on aerosol metal solubility and deposition velocities are element-specific. As shown in Fig. 5, the transport processes enhance the solubilities of all elements under all leaching protocols and the enhancement extent increases with lithotendency. Based on the data of size specific solubilities and masses obtained in this study (Table 1, last column), the average deposition velocities varied significantly among different elements, ranging from a few folds to one order of magnitude, which are 0.04–0.43, 0.08–0.49, 0.20–0.63, and 0.19–0.80 cm s^{-1} for ultrapure water, buffer, Berger, and total leaching treatments, respectively (Table 1). However, while separating the size-fractionated aerosols to two fractions (fine and coarse), the velocities are relatively constrained either for fine or coarse size aerosols (Table 1), in which the velocities are 0.013–0.030, 0.015–0.033, 0.018–0.037, and 0.022–0.047 among the elements for fine fraction; and 0.73–0.90, 0.84–0.98, 0.90–1.0, and 0.92–1.0 cm s^{-1} for coarse fraction, respectively. Due to extremely low deposition velocities of fine aerosol, the effects of the deviation of the fine aerosol velocities for total flux estimate would be further reduced. In brief, two-size aerosol sampling provides a much more reliable flux estimate for aerosol metal deposition than total suspended particle sampling. Without knowing the metal mass fraction in multiple size-fractionated aerosols, one may use two-size deposition velocities to obtain more accurate estimates for aerosol metal fluxes. Since it is highly challenging to obtain sufficient multiple size aerosols onboard due to cruise time limitation and low aerosol mass over the open ocean, for related studies in other major oceanic regions, we suggest to carry out multiple size-fractionated aerosol sampling on an islet as this study first to obtain the value of region specific deposition velocities for flux estimates. These velocities can then be used to obtain region representative deposition velocities for 1-size or 2-size sampling. In terms of solubility applied to global model flux estimates, we think that ultrapure water leach underestimates the aerosol solubility of V, Al, Fe, and Ti in the surface water of the ECS. The buffer and Berger leaches are more realistic to represent the metal solubility in the ocean.

Data availability

Data will be made available on request.

Acknowledgments

We appreciate the technical assistance of H.-Y. Chen for ECS aerosol sampling in this study. This study was financially supported by grants 108-2611-M-001-006-MY3 and 111-2611-M-001 -006 -MY3 from National Science and Technology Council and Investigator Award AS-IA-110-M03 from Academia Sinica to T.-Y. Ho.

Appendix A. Supplementary data

Supplementary data to this article can be found online at https://doi.org/10.1016/j.marchem.2023.104268.

References

ATSDR, 1999. Toxicological profile for cadmium. U.S. Department of Health and Human Services. Public Health Service. Agency for Toxic Substances and Disease Registry.

Baker, A.R., Jickells, T.D., 2006. Mineral particle size as a control on aerosol iron solubility. Geophys. Res. Lett. 33 (17) https://doi.org/10.1029/2006gl026557.

Baker, A.R., Jickells, T.D., Witt, M., Linge, K.L., 2006. Trends in the solubility of iron, aluminium, manganese and phosphorus in aerosol collected over the Atlantic Ocean. Mar. Chem. 98 (1), 43–58. https://doi.org/10.1016/j.marchem.2005.06.004.

Baker, A.R., et al., 2016. Trace element and isotope deposition across the air-sea interface: progress and research needs. Philos. Trans. A Math. Phys. Eng. Sci. 374 (2081) https://doi.org/10.1098/rsta.2016.0190.

Baker, A.R., et al., 2021. Changing atmospheric acidity as a modulator of nutrient deposition and ocean biogeochemistry. Sci. Adv. 7 (28) https://doi.org/10.1126/sciadv.abd8800.

Berger, C.J.M., Lippiatt, S.M., Lawrence, M.G., Bruland, K.W., 2008. Application of a chemical leach technique for estimating labile particulate aluminum, iron, and manganese in the Columbia River plume and coastal waters off Oregon and Washington. J. Geophys. Res. 113 https://doi.org/10.1029/2007jc004703.

Bonnet, S., Guieu, C., 2004. Dissolution of atmospheric iron in seawater. Geophys. Res. Lett. 31 (3) https://doi.org/10.1029/2003gl018423.

Buck, C.S., Landing, W.M., Resing, J.A., Lebon, G.T., 2006. Aerosol iron and aluminum solubility in the northwest Pacific Ocean: results from the 2002 IOC cruise. Geochem. Geophys. Geosyst. 7 (4) https://doi.org/10.1029/2005gc000977.

Chen, C.C., et al., 2022. Nickel superoxide dismutase protects nitrogen fixation in Trichodesmium. Limnol. Oceanogr. Lett. 7 (4), 363–371. https://doi.org/10.1002/lol2.10263.

Cheng, M.-C., You, C.-F., Cao, J., Jin, Z., 2012. Spatial and seasonal variability of water-soluble ions in PM2.5 aerosols in 14 major cities in China. Atmos. Environ. 60, 182–192. https://doi.org/10.1016/j.atmosenv.2012.06.037.

Clough, R., Lohan, M.C., Ussher, S.J., Nimmo, M., Worsfold, P.J., 2019. Uncertainty associated with the leaching of aerosol filters for the determination of metals in aerosol particulate matter using collision/reaction cell ICP-MS detection. Talanta 199, 425–430. https://doi.org/10.1016/j.talanta.2019.02.067.

Cutter, G., et al., 2017. Sampling and Sample-Handling Protocols for GEOTRACES Cruises, 3. https://doi.org/10.25607/OBP-2.

Duce, R.A., et al., 1991. The atmospheric input of trace species to the world ocean. Glob. Biogeochem. Cycles 5 (3), 193–259. https://doi.org/10.1029/91gb01778.

Eggimann, D.W., Betzer, P.R., 1976. Decomposition and analysis of refractory oceanic suspended materials. Anal. Chem. 48 (6), 886–890. https://doi.org/10.1021/ac60370a005.

Félix-Bermúdez, A., Delgadillo-Hinojosa, F., Torres-Delgado, E.V., Muñoz-Barbosa, A., 2020. Does sea surface temperature affect solubility of iron in mineral dust? The Gulf of California as a case study. J. Geophys. Res. Oceans 125 (9). https://doi.org/10.1029/2019jc015999.

Fishwick, M.P., et al., 2014. The impact of changing surface ocean conditions on the dissolution of aerosol iron. Glob. Biogeochem. Cycles 28 (11), 1235–1250. https://doi.org/10.1002/2014gb004921.

Fishwick, M.P., et al., 2018. Impact of surface ocean conditions and aerosol provenance on the dissolution of aerosol manganese, cobalt, nickel and lead in seawater. Mar. Chem. 198, 28–43. https://doi.org/10.1016/j.marchem.2017.11.003.

Foret, G., Bergametti, G., Dulac, F., Menut, L., 2006. An optimized particle size bin scheme for modeling mineral dust aerosol. J. Geophys. Res. 111 (D17) https://doi.org/10.1029/2005jd006797.

Gunchin, G., Osan, J., Migliori, A., Shagjjamba, D., Streli, C., 2021. Chromium and zinc speciation in airborne particulate matter collected in Ulaanbaatar, Mongolia, by X-ray absorption near-edge structure spectroscopy. Aerosol Air Qual. Res. 21 (8) https://doi.org/10.4209/aaqr.210018.

Ho, T.Y., et al., 2003. The elemental composition of some marine phytoplankton. J. Phycol. 39 (6), 1145–1159. https://doi.org/10.1111/j.0022-3646.2003.03-090.x.

Hsieh, C.-C., Chen, H.-Y., Ho, T.-Y., 2022. The effect of aerosol size on Fe solubility and deposition flux: a case study in the East China Sea. Mar. Chem. 241 https://doi.org/10.1016/j.marchem.2022.104106.

Hu, Z.C., Gao, S., 2008. Upper crustal abundances of trace elements: a revision and update. Chem. Geol. 253 (3–4), 205–221. https://doi.org/10.1016/j.chemgeo.2008.05.010.

Jickells, T.D., et al., 2005. Global iron connections between desert dust, ocean biogeochemistry, and climate. Science 308 (5718), 67–71. https://doi.org/10.1126/science.1105959.

Jickells, T.D., Baker, A.R., Chance, R., 2016. Atmospheric transport of trace elements and nutrients to the oceans. Philos. Trans. A Math. Phys. Eng. Sci. 374 (2081) https://doi.org/10.1098/rsta.2015.0286.

Kessler, N., Kraemer, S.M., Shaked, Y., Schenkeveld, W.D.C., 2020. Investigation of siderophore-promoted and reductive dissolution of dust in marine microenvironments such as *Trichodesmium* colonies. Front. Mar. Sci. 7 https://doi.org/10.3389/fmars.2020.00045.

Li, W., et al., 2017. Air pollution-aerosol interactions produce more bioavailable iron for ocean ecosystems. Sci. Adv. 3 (3) https://doi.org/10.1126/sciadv.1601749 e1601749.

Li, R., et al., 2023. Evaluating the effects of contact time and leaching solution on measured solubilities of aerosol trace metals. Appl. Geochem. 148 https://doi.org/10.1016/j.apgeochem.2022.105551.

Longo, A.F., et al., 2016. Influence of atmospheric processes on the solubility and composition of Iron in Saharan dust. Environ. Sci. Technol. 50 (13), 6912–6920. https://doi.org/10.1021/acs.est.6b02605.

Mackey, K.R., Chien, C.T., Post, A.F., Saito, M.A., Paytan, A., 2015. Rapid and gradual modes of aerosol trace metal dissolution in seawater. Front. Microbiol. 5, 794. https://doi.org/10.3389/fmicb.2014.00794.

Mahowald, N.M., et al., 2005. Atmospheric global dust cycle and iron inputs to the ocean. Glob. Biogeochem. Cycles 19 (4). https://doi.org/10.1029/2004gb002402 n/a-n/a.

Martin, J.H., Fitzwater, S.E., 1988. Iron deficiency limits phytoplankton growth in the north-east Pacific subarctic. Nature 331 (6154), 341–343. https://doi.org/10.1038/331341a0.

Meskhidze, N., et al., 2019. Perspective on identifying and characterizing the processes controlling iron speciation and residence time at the atmosphere-ocean interface. Mar. Chem. 217 https://doi.org/10.1016/j.marchem.2019.103704.

Morel, F.M.M., Lam, P.J., Saito, M.A., 2020. Trace metal substitution in marine phytoplankton. Annu. Rev. Earth Planet. Sci. 48 (1), 491–517. https://doi.org/10.1146/annurev-earth-053018-060108.

Morton, P.L., et al., 2013. Methods for the sampling and analysis of marine aerosols: results from the 2008 GEOTRACES aerosol intercalibration experiment. Limnol. Oceanogr. Methods 11 (2), 62–78. https://doi.org/10.4319/lom.2013.11.62.

Myriokefalitakis, S., et al., 2018. Reviews and syntheses: the GESAMP atmospheric iron deposition model intercomparison study. Biogeosciences 15 (21), 6659–6684. https://doi.org/10.5194/bg-15-6659-2018.

Nicholls, G.D., 1963. Environmental studies in sedimentary geochemistry. Sci. Prog. 51 (201), 12–31.

Ohta, A., et al., 2006. Chemical compositions and XANES speciations of Fe, Mn and Zn from aerosols collected in China and Japan during dust events. Geochem. J. 40 (4), 363–376. https://doi.org/10.2343/geochemj.40.363.

Paytan, A., et al., 2009. Toxicity of atmospheric aerosols on marine phytoplankton. Proc. Natl. Acad. Sci. U. S. A. 106 (12), 4601–4605. https://doi.org/10.1073/pnas.0811486106.

Perron, M.M.G., et al., 2020. Assessment of leaching protocols to determine the solubility of trace metals in aerosols. Talanta 208, 120377. https://doi.org/10.1016/j.talanta.2019.120377.

Raiswell, R., Canfield, D.E., 2012. The Iron biogeochemical cycle past and present. Geochem. Perspect. 1 (1), 1–220. https://doi.org/10.7185/geochempersp.1.1.

Sakata, K., et al., 2014. Identification of sources of lead in the atmosphere by chemical speciation using X-ray absorption near-edge structure (XANES) spectroscopy. J. Environ. Sci. 26 (2), 343–352. https://doi.org/10.1016/s1001-0742(13)60430-1.

Sakata, K., et al., 2022. Iron (Fe) speciation in size-fractionated aerosol particles in the Pacific Ocean: The role of organic complexation of Fe with humic-like substances in controlling Fe solubility. Atmos. Chem. Phys. 22 (14), 9461–9482. https://doi.org/10.5194/acp-22-9461-2022.

Sakata, K., Sakaguchi, A., Yokoyama, Y., Terada, Y., Takahashi, Y., 2017. Lead speciation studies on coarse and fine aerosol particles by bulk and micro X-ray absorption fine structure spectroscopy. Geochem. J. 51 (3), 215–225. https://doi.org/10.2343/geochemj.2.0456.

Sarthou, G., et al., 2003. Atmospheric iron deposition and sea-surface dissolved iron concentrations in the eastern Atlantic Ocean. Deep-Sea Res. I Oceanogr. Res. Pap. 50 (10–11), 1339–1352. https://doi.org/10.1016/s0967-0637(03)00126-2.

Seinfeld, J.H., Pandis, S.N., 2016. Atmospheric Chemistry and Physics: From Air Pollution to Climate Change, 3rd. Wiley-interscience, p. 1326.

Shelley, R.U., Morton, P.L., Landing, W.M., 2015. Elemental ratios and enrichment factors in aerosols from the US-GEOTRACES North Atlantic transects. Deep-Sea Res. II Top. Stud. Oceanogr. 116, 262–272. https://doi.org/10.1016/j.dsr2.2014.12.005.

Shelley, R.U., Landing, W.M., Ussher, S.J., Planquette, H., Sarthou, G., 2018. Regional trends in the fractional solubility of Fe and other metals from North Atlantic aerosols (GEOTRACES cruises GA01 and GA03) following a two-stage leach. Biogeosciences 15 (7), 2271–2288. https://doi.org/10.5194/bg-15-2271-2018.

Shi, Z.B., et al., 2012. Impacts on iron solubility in the mineral dust by processes in the source region and the atmosphere: a review. Aeolian Res. 5, 21–42. https://doi.org/10.1016/j.aeolia.2012.03.001.

Slinn, S.A., Slinn, W.G.N., 1980. Predictions for particle deposition on natural waters. Atmos. Environ. (1967) 14 (9), 1013–1016. https://doi.org/10.1016/0004-6981(80)90032-3.

Takahashi, Y., Higashi, M., Furukawa, T., Mitsunobu, S., 2011. Change of iron species and iron solubility in Asian dust during the long-range transport from western China to Japan. Atmos. Chem. Phys. 11 (21), 11237–11252. https://doi.org/10.5194/acp-11-11237-2011.

Wang, B.-S., Ho, T.-Y., 2020. Aerosol Fe cycling in the surface water of the northwestern Pacific Ocean. Prog. Oceanogr. 183 https://doi.org/10.1016/j.pocean.2020.102291.

Wu, H.-Y., Hsieh, C.-C., Ho, T.-Y., 2023. Trace Metal Dissolution Kinetics of East Asian Size-Fractionated Aerosols in Seawater: The Effect of a Model Siderophore unpublished manuscript.